Chaotic Induced-Charge Electro-Osmosis

Scott M. Davidson, Mathias B. Andersen, and Ali Mani*
Center for Turbulence Research, Stanford University, Stanford, California 94305, USA
Department of Mechanical Engineering, Stanford University, Stanford, California 94305, USA
(Received 16 October 2013; revised manuscript received 20 December 2013; published 24 March 2014)

We present direct numerical simulations of the coupled Poisson-Nernst-Planck and Navier-Stokes equations for an electrolyte around a polarizable cylinder subject to an external electric field. For high fields, a novel chaotic flow phenomenon is discovered. Our calculations indicate significant improvement in the prediction of the mean flow relative to standard asymptotic models. These results open possibilities for chaos-enhanced mixing in microdevices and provide insight into barriers to efficient electrokinetic micropumps with broad applications in electrochemical and lab-on-a-chip systems.

DOI: 10.1103/PhysRevLett.112.128302 PACS numbers: 47.57.jd, 47.52.+j

Induced-charge electro-osmosis (ICEO) refers to flows driven by electrostatic forces arising from the action of an applied electric field on free charge induced by the field itself in microscopically thin boundary layers on the surface of a polarizable object [1,2]. Within the last decade, ICEO has received considerable attention as a means for mixing and pumping in microfluidic lab-on-a-chip systems, which are typically used for biochemical analysis [3].

In the late 1990s, Ramos and co-workers discovered ac electro-osmosis [4], a variant of ICEO used for pumping in microchannels. Some years later, a more general theoretical description of ICEO, including both ac and dc variants, was developed by Bazant and Squires [5,6]. Figure 1 presents a canonical ICEO problem showing an ideally polarizable cylinder fixed in a binary aqueous electrolyte. An external electric field E_b drives ions in the bulk and polarizes the cylinder, which in turn leads to the formation of a surface charge and screening electric double layers (EDLs) on the cylinder. Ignoring surface conduction and assuming uniform bulk conductivity, Bazant and Squires computed the tangential electric field outside of the EDLs to be $E_\theta = -2E_b \sin(\theta)$. Given the fixed potential of the cylinder, the induced zeta potential across the thin EDLs was computed to be $\zeta = 2E_b a \cos(\theta)$. Using the Helmholtz-Smoluchowski relation [7], they predicted that the tangential field acting on the EDL should lead to an induced slip velocity with quadratic dependence on the electric field $U \sim E_b^2$. The quadratic dependence of the induced flow in ICEO offered promising advantages over linear electro-osmotic flow systems, namely, flow rates faster than linear electro-osmosis at high voltages and a net flow even under ac forcing, thus avoiding electrode reactions or bubble formation.

However, after recent comparisons with experimental measurements, it became clear that ICEO velocities in practice are lower than those predicted by the weakly nonlinear asymptotic model of Bazant and Squires [5]. Particularly at high voltages, the discrepancy can be up to an order of magnitude [8–11], almost neutralizing the advantage of the quadratic scaling of ICEO velocities and leaving open the question of whether ICEO or linear electro-osmosis is a more efficient means of generating microscale flows.

To explain this discrepancy, several modifications have been proposed. The majority of the papers in the literature have attributed the differences to noncontinuum effects [12] and have attempted to provide better fits to the experimental data by invoking models taking into account corrections such as the Stern layer and ion packing near the surface [13]. However, to capture the correct magnitude of ICEO velocities, these models have resorted to unphysical choices of tunable parameters such as Stern layer thicknesses or ion volumes at least an order of magnitude too large [10,13]. Most recently, asymptotic models [14] and numerical simulations [15] have been developed to take into account effects of surface conduction and bulk concentration polarization. These models, however, only solve steady equations, thereby mathematically eliminating the possibility of flow instability and unsteadiness.

In this Letter, we present direct numerical simulations (DNS) of the ICEO phenomenon through solution of the

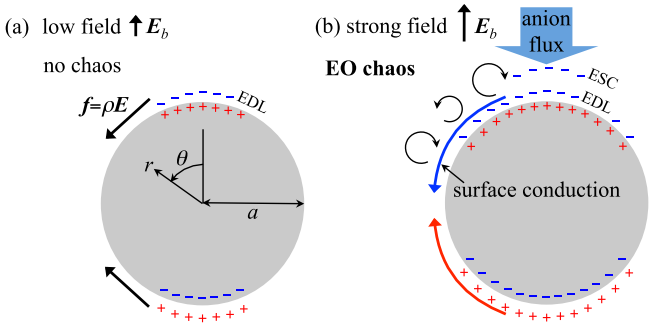

FIG. 1 (color online). Schematic of key elements of ICEO in a binary electrolyte around an ideally polarizable cylinder subject to an external electric field E_b. (a) Low field. (b) High field.

Navier-Stokes and Poisson-Nernst-Planck equations. Our simulations resolve the thin EDLs and fast bulk charge-relaxation time without resorting to any asymptotic simplification. We show that at large fields, ICEO presents nonlinear and chaotic dynamics with $O(1)$ spatiotemporal fluctuations in all variables. The effect on the time-averaged kinematics is a retardation of the flow velocity, and our finding therefore offers an explanation for the discrepancy between theory and experiment in ICEO without resorting to any tunable parameter. We study the canonical ICEO system of an infinitely long 2D metallic cylinder in an aqueous binary electrolyte subject to an applied dc electric field. We have performed other preliminary studies that confirm that chaotic dynamics also exist in ac fields. While the present results from our dc-forced DNS succinctly capture the basic picture of chaotic ICEO, we defer a presentation of more elaborate ac-forced DNS to a future publication with a wider scope.

Basic physical picture.—Figure 1 depicts the basic mechanism of the electro-osmotic flow due to an induced charge on a polarizable cylinder. The figure contrasts two scenarios involving low and high electric fields, with the key difference being the relative importance of surface-conduction-induced concentration polarization [7].

Surface conduction describes current carried by the excess ions in the EDL and is quantified in dimensionless form by the Dukhin number Du [7]. In the low-field limit, one can show that Du scales as E_b^2, and, as discussed by Squires and Bazant [6], surface conduction can be safely ignored. However, as the external field increases, the relative effect of surface conduction becomes increasingly important due to the higher charge stored in the EDLs. As shown in Fig. 1(b), this tangential transport of counterions needs to be supplied from the neutral bulk via a flux normal to the EDL [16]. This selective intake of counterions normal to the surface leads to the concentration-polarization phenomenon [7,17] defined by ion depletion near the ion-absorption interfaces ($\theta = 0°$, 180°) and ion enrichment near the ejection interfaces ($\theta = \pm 90°$) [16].

In the high voltage limit, concentration-polarization depletion can lead to the formation of a nonequilibrium charged layer between the EDL and the electroneutral bulk called the extended space charge region (ESC) [17–20]. Transport and dynamics of ESC has been long studied in the context of ion-selective membrane science. These theoretical and experimental studies confirm that the ESC can be hydrodynamically unstable [21–25]. Particularly, our recent study presents the first DNS of concentration-polarization-induced chaos next to ion-selective membranes [26]. Figure 2 shows the charge density field and the concentration boundary layer structure just below the onset voltage of instability. Figure 2(b) shows that for $E_b a$ of 30 thermal volts, a thick extended space charge region is developed between the classically known EDL and electroneutral bulk regions. Next, we

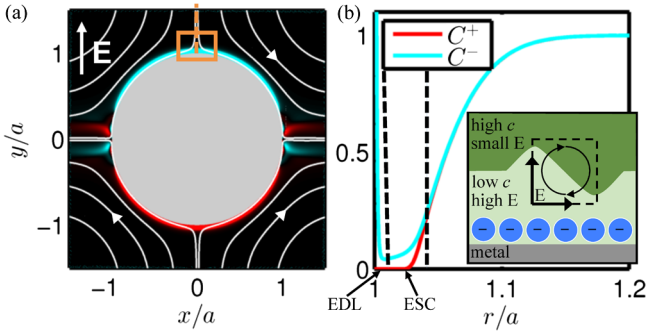

FIG. 2 (color online). Results from a stable solution for $E_b a/V_T = 30$ showing (a) a contour plot of the charge density (negative = blue, positive = red), and (b) anion and cation concentration versus radial distance along the dashed line indicated in (a). The inset is a zoomed schematic on the area indicated by the rectangle in (a) showing a hypothetical vortex and the resulting perturbation to the concentration contours.

describe how the presence of charge away from the wall due to the ESC can lead to a positive feedback mechanism sustaining the instability. The inset of Fig. 2(b) shows a clockwise-rotating hypothetical vortex near the ESC with the corresponding perturbations to the salt concentration field. For this qualitative argument, we track only one isocontour of concentration. The high-concentration zone, due to its low Ohmic resistance, is expected to have a relatively more uniform potential, and thus a smaller electric field, which we neglect. Given the upward background field, we examine the circulation of the electric field around the test loop indicated by the dashed square. Since this circulation must be zero, a tangential field must be induced from left to right close to the surface. This tangential field acts on the negatively charged ESC, producing a body force in a direction amplifying the hypothetical vortex. For sufficiently large fields, this feedback loop can overcome viscous dissipation and lead to overall growth of the perturbing vortices. The role of the ESC is crucial in the sense that it provides charge well into the bulk.

Governing equations.—Our starting point is the incompressible Navier-Stokes and Poisson-Nernst-Planck equations for a symmetric binary electrolyte in the dilute limit

$$\rho\left[\frac{\partial \boldsymbol{v}}{\partial t} + (\boldsymbol{v}\cdot\nabla)\boldsymbol{v}\right] = -\nabla p + \mu\nabla^2\boldsymbol{v} + \rho_e\boldsymbol{E}, \tag{1a}$$

$$\nabla\cdot\boldsymbol{v} = 0, \tag{1b}$$

$$\frac{\partial c^{\pm}}{\partial t} + \boldsymbol{v}\cdot\nabla c^{\pm} = D\nabla\cdot(\nabla c^{\pm} \pm V_T^{-1}c^{\pm}\nabla\phi), \tag{1c}$$

$$-\varepsilon\nabla^2\phi = \rho_e, \tag{1d}$$

in which $\boldsymbol{v}$, p, c^+, c^-, and ϕ are the fluid velocity, hydrodynamic pressure, cation concentration, anion

concentration, and electrostatic potential, respectively. Moreover, $\boldsymbol{E} = -\nabla\phi$ is the electric field, $\rho_e = ze(c^+ - c^-)$ is the free charge density, and ρ, μ, D, $V_T = k_B T/(ze)$, ϵ, and z are the fluid mass density, fluid viscosity, ionic diffusivity, thermal voltage, dielectric permittivity, and ionic valence, respectively. Finally, e, k_B, and T are the elementary charge, Boltzmann constant, and temperature, respectively.

These equations are solved in 2D around a metallic cylinder. The boundary conditions on the cylinder ($r = a$) are no flux, no slip, no penetration, and fixed potential. In the far field, we enforce fixed concentration $c^+ = c^- = c_0$, zero flow, and uniform electric field E_b. The typical domain size is taken to be $\approx 100a$ to ensure independence of the results from the boundary location.

The dimensionless parameters of the problem are the electrohydrodynamic coupling constant $\kappa = \varepsilon V_T^2/(\mu D)$, the Schmidt number $\mathrm{Sc} = \mu/(\rho D)$, the dimensionless applied field $E_b a/V_T$, and the dimensionless Debye length $\epsilon = \lambda_D/a$, where $\lambda_D = \sqrt{\varepsilon k_B T/[2(ze)^2 c_0]}$ is the dimensionful Debye length.

In this Letter, we consider $\kappa = 0.5$ and $\mathrm{Sc} = 1000$ consistent with typical aqueous electrolytes. The applied field is varied from $E_b a/V_T \ll 1$ up to 50. ϵ is taken to be equal to $\epsilon = 10^{-3}$ (e.g., representing a 20–μm-diameter cylinder in a 1-mM electrolyte).

The governing equations are solved using second-order finite differences in cylindrical coordinates on a staggered mesh. To this end, we have developed a specialized parallel code with several features, including nondissipative numerical advection and use of fast Fourier transforms for fast solution of the elliptic equations. Furthermore, we have verified that the nonlinear inertial term $(\boldsymbol{v}\cdot\nabla)\boldsymbol{v}$ in the Navier-Stokes equation (1a) is negligible due to the small Reynolds number of the flow, and we have neglected this term in the computations. The accuracy of our numerical algorithm has been extensively verified using the method of manufactured solution against a class of generalized exact solutions capable of verifying the second-order accuracy of all terms [26,27]. The numerical mesh consists of 768 points uniformly spaced in the azimuthal direction and 400 mesh points in the radial direction, with the smallest mesh size equal to $10^{-5}a$ on the surface (sufficient to resolve the EDL) and gradually stretched away from the cylinder with a uniform stretching factor of $\approx 3\%$.

Results.—Our DNS calculations indicate that instability and chaos can develop in ICEO with a significant impact on the system-level response. Furthermore, these results are unlikely to have been discovered using purely asymptotic methods, as has been the tradition in the field of electrokinetics.

Figure 3 shows snapshots of the dimensionless salt concentration $c = (c^+ + c^-)/(2c_0)$ (top row) and the dimensionless free charge density $(c^+ - c^-)/c_0$ (bottom row) separated in time by $5 \times 10^{-4} a^2/D = 0.5 a\lambda_D/D$, i.e., half of the RC time of the system [28]. In the Supplemental Material [29], we present movies from these simulations as well as time spectra of velocity and concentration fluctuations. These spectra are broadband, indicating the presence of fluctuations over a wide range of time scales and confirming the chaotic nature of the phenomenon.

The streamlines show that chaotic vortices are generated at $\theta = 0°$, 180° and advected with the background flow towards $\theta = \pm 90°$, where they are ejected back to the bulk, thus forming a fascinating four-way shedding phenomenon around the cylinder. The top row of Fig. 3 shows that relatively large ion-depleted voids of size $O(0.1a)$ are formed at $\theta = 0°$, 180° and subsequently advected towards $\theta = \pm 90°$. These voids are formed due to vortices transporting depleted fluid into the bulk.

Enrichment jets with peak concentration $O(10)$ are due to surface conduction carrying counterions through the highly enriched EDLs and their ejection at $\theta = \pm 90°$.

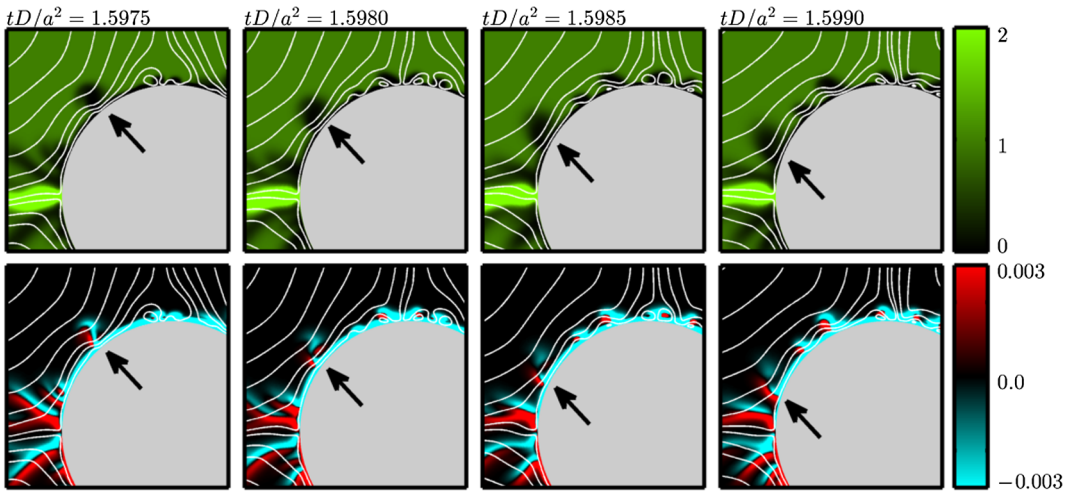

FIG. 3 (color online). Instantaneous snapshots of the dimensionless salt concentration (top row) and the dimensionless free charge density (bottom row) with flow streamlines superposed for $\epsilon = 10^{-3}$ and $E_b a/V_T = 50$. The arrows track a single void.

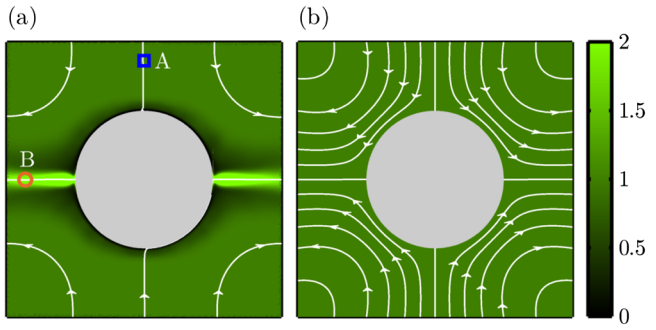

FIG. 4 (color online). Color plots of the time-averaged salt concentration and flow streamlines for $E_b a/V_T = 50$, highlighting the difference in ICEO calculations by (a) the DNS and (b) the weakly nonlinear asymptotic model. Velocity versus voltage is plotted in Fig. 5 for points A and B located at $r = \sqrt{3}a$ and $\theta = 0°$ and 90°. (a) Time-Averaged DNS. (b) Asymptotic.

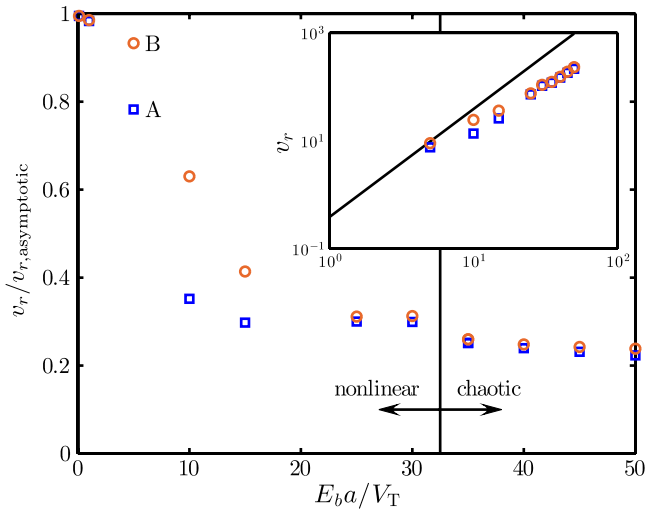

FIG. 5 (color online). Magnitude of the mean radial velocity v_r from our DNS scaled by the radial velocity $v_{r,\text{asymptotic}}$ from the weakly nonlinear asymptotic model at probes A (blue squares) and B (orange circles) as a function of applied field $E_b a/V_T$. Inset: As in the main panel, but without scaling, and with $v_{r,\text{asymptotic}}$ given by the black line. The positions of probes A (inflow) and B (outflow) are indicated in Fig. 4.

It should be noted that the surface conduction inside of the EDLs is well resolved in our calculations but that the EDLs are not visually observable since they are much thinner than the scales captured in the figure.

The bottom row of panels in Fig. 3 shows interesting features in the charge density. The results indicate that the structure of the ESC is broken by chaotic vortices, leading to an ESC with a highly unsteady and irregular boundary. For this specific calculation, the maximum charge density in the ESC is $O(10^{-1})$. Wherever there is a void, there is a corresponding zone of bulk charge of $O(10^{-2})$ within that region that is advected along the surface. As they approach $\theta = \pm 90°$, the structures are stretched into ribbonlike shapes with bands of positive and negative charge.

Figure 4 shows color plots of the time-averaged concentration and flow streamlines from our DNS [Fig. 4(a)] in contrast to the weakly nonlinear asymptotic model [Fig. 4(b)]. Squires and Bazant calculated the asymptotic velocity field as $\{v_r, v_\theta\} = 2U_0(a/r)^3\{\cos(2\theta), \sin(2\theta)\}$, where $U_0 = \epsilon a E_b^2/\mu$ [6]. While the asymptotic model displays uniform concentration and symmetric streamlines, the DNS shows strong concentration polarization around the cylinder (even after time averaging) with ion depletion starting at $\theta = 0°$, 180° and advecting towards $\theta = \pm 90°$. Furthermore, a strong salt enrichment jet due to ejection of ions via the surface-conduction mechanism is predicted. A similar enrichment phenomenon near metallic posts was observed experimentally by Leinweber *et al.* [30].

The difference in the streamlines in Fig. 4 indicates the difference between the flow fields with the spacing between streamlines being inversely proportional to velocity. The time-averaged flow from the DNS is much smaller than that from the weakly nonlinear asymptotic model by a factor up to ≈5.

Figure 5 shows the effect of chaos on the predicted radial velocity magnitude. The retardation of the DNS velocity from the asymptotic scaling develops rapidly in the nonlinear regime but levels off around $E_b a/V_T = 25$. The DNS also predicts asymmetry between the inward and the outward velocities by up to a factor of about 2 in the nonlinear regime that is not captured by the asymptotic model. Above ≈30 thermal volts, the DNS becomes chaotic and the gap between the DNS and the weakly nonlinear asymptotic model further increases. In the chaotic regime, mean velocities from the DNS are compared to the steady asymptotic prediction. From the inset in Fig. 5, it is evident that in the chaotic regime, the velocity still scales very nearly like E_b^2, even though the predicted velocities are significantly lower than those from the asymptotic analysis. This is consistent with the experimental evidence by Harnett *et al.* [9] who measured ICEO flow velocities 4 times smaller than those predicted by their (slightly improved) asymptotic model.

Summary.—We presented results from direct solutions to the Poisson-Nernst-Planck and Navier-Stokes equations for a binary electrolyte next to a polarizable object. Our DNS shows for the first time that induced-charge electrokinetic systems can be chaotic at high voltages. The resulting nonlinear dynamics due to concentration polarization are shown to significantly suppress the time-averaged ICEO flow and can explain existing puzzling discrepancies between asymptotic-based models and measurements. These results are directly relevant to applications such as pumping and mixing in microdevices. Flow chaos and unsteadiness may be either beneficial (mixing) or deleterious (pumping), and the presented insights can guide design to either enhance or suppress them. Additionally, this newly discovered instability may be present in a broad range of

electrochemical applications in which aqueous electrolytes are forced by electric fields near electrodes, including electrolysis and electrodeposition.

Our DNS database can be used to guide the improvement of asymptotic models needed for design and optimization studies. Plausible extensions of this work include the investigation of ac fields and the coupling of chaos with steric effects. The results from this study present novel implications in the fields of electrokinetics, electrochemistry, and microfluidics and offer opportunities for interactions between chemical engineers, fluid dynamicists, and applied mathematicians.

The authors would like to thank Professor Martin Z. Bazant and Professor Andreas Acrivos for their comments. This material is based upon work supported by the National Science Foundation Graduate Research Fellowship under Grant No. DGE-114747. S. M. D. is supported by a Robert and Katherine Eustis Stanford Graduate Fellowship. We gratefully acknowledge support from the Charles Lee Powell Foundation.

*alimani@stanford.edu

[1] M. Z. Bazant and T. M. Squires, Curr. Opin. Colloid Interface Sci. **15**, 203 (2010).
[2] M. Z. Bazant, in *Electrokinetics and Electrohydrodynamics in Microsystems*, CISM Courses and Lectures Vol. 530, edited by A. Ramos (Springer, Vienna, 2011) p. 221.
[3] T. M. Squires and S. R. Quake, Rev. Mod. Phys. **77**, 977 (2005).
[4] A. Ramos, H. Morgan, N. G. Green, and A. Castellanos, J. Phys. D **31**, 2338 (1998).
[5] M. Z. Bazant and T. M. Squires, Phys. Rev. Lett. **92**, 066101 (2004).
[6] T. M. Squires and M. Z. Bazant, J. Fluid Mech. **509**, 217 (2004).
[7] J. Lyklema, *Fundamentals of Interface and Colloid Science—Solid-Liquid Interfaces* (Academic, London, 1995), Vol. 2.
[8] J. A. Levitan, S. Devasenathipathy, V. Studer, Y. Ben, T. Thorsen, T. M. Squires, and M. Z. Bazant, Colloids Surf. A **267**, 122 (2005).
[9] C. K. Harnett, J. Templeton, K. A. Dunphy-Guzman, Y. M. Senousy, and M. P. Kanouff, Lab Chip **8**, 565 (2008).
[10] M. Z. Bazant, M. S. Kilic, B. D. Storey, and A. Ajdari, Adv. Colloid Interface Sci. **152**, 48 (2009).
[11] C. Canpolat, S. Qian, and A. Beskok, Microfluid. Nanofluid. **14**, 153 (2013).
[12] M. Z. Bazant, B. D. Storey, and A. A. Kornyshev, Phys. Rev. Lett. **106**, 046102 (2011).
[13] B. D. Storey, L. R. Edwards, M. S. Kilic, and M. Z. Bazant, Phys. Rev. E **77**, 036317 (2008).
[14] O. Schnitzer and E. Yariv, Phys. Rev. E **86**, 061506 (2012).
[15] M. M. Gregersen, M. B. Andersen, G. Soni, C. Meinhart, and H. Bruus, Phys. Rev. E **79**, 066316 (2009).
[16] K. T. Chu and M. Z. Bazant, Phys. Rev. E **74**, 011501 (2006).
[17] S. Dukhin, Adv. Colloid Interface Sci. **35**, 173 (1991).
[18] W. H. Smyrl and J. Newman, Trans. Faraday Soc. **63**, 207 (1967).
[19] S. Barany, N. A. Mishchuk, and D. C. Prieve, J. Colloid Interface Sci. **207**, 240 (1998).
[20] L. Højgaard Olesen, M. Z. Bazant, and H. Bruus, Phys. Rev. E **82**, 011501 (2010).
[21] S. M. Rubinstein, G. Manukyan, A. Staicu, I. Rubinstein, B. Zaltzman, R. G. H. Lammertink, F. Mugele, and M. Wessling, Phys. Rev. Lett. **101**, 236101 (2008).
[22] G. Yossifon and H.-C. Chang, Phys. Rev. Lett. **101**, 254501 (2008).
[23] B. Zaltzman and I. Rubinstein, J. Fluid Mech. **579**, 173 (2007).
[24] E. A. Demekhin, V. S. Shelistov, and S. V. Polyanskikh, Phys. Rev. E **84**, 036318 (2011).
[25] A. S. Khair, Phys. Fluids **23**, 072003 (2011).
[26] C. L. Druzgalski, M. B. Andersen, and A. Mani, Phys. Fluids **25**, 110804 (2013).
[27] K. Salari and P. Knupp, Sandia National Laboratories Technical Report No. SAND2000-1444, 2000.
[28] M. Z. Bazant, K. Thornton, and A. Ajdari, Phys. Rev. E **70**, 021506 (2004).
[29] See Supplemental Material at http://link.aps.org/supplemental/10.1103/PhysRevLett.112.128302 for movies showing the concentration and charge density fields at various applied voltages and plots of temporal spectra of fluctuating velocity and concentration.
[30] F. C. Leinweber, J. C. T. Eijkel, J. G. Bomer, and A. van den Berg, Anal. Chem. **78**, 1425 (2006).